

## Simulation and Investigation of Si-Based Piezoelectric Micromachined Ultrasonic Transducer (PMUT) Performances

H. Aris<sup>1,2,\*</sup>, Muhammad Nizam Bin Rosli<sup>1</sup>, M. N. M. Nuzaihan<sup>3</sup>, Z. Sauli<sup>1,2</sup>, W.M.W. Norhaimi<sup>1,2</sup>

<sup>1</sup>Faculty of Electronic Engineering & Technology, Universiti Malaysia Perlis (UniMAP), 02600 Arau, Perlis, Malaysia.

<sup>2</sup>Centre of Excellence for Micro System Technology (MiCTEC), Universiti Malaysia Perlis (UniMAP), 02600 Arau, Perlis, Malaysia

<sup>3</sup>Institute of Nano Electronic Engineering (INEE), Universiti Malaysia Perlis (UniMAP), 02600 Arau, Perlis, Malaysia.

Received 29 August 2022, Revised 13 September 2022, Accepted 9 August 2023

### ABSTRACT

*Micro-electromechanical system (MEMS) based piezoelectric ultrasonic transducers for acoustic imaging of the surroundings are known as piezoelectric micromachined ultrasonic transducers (PMUTs). This research proposes a structural design of the PMUT with four fixed-guided beams. The beam is subjected to lateral loads, with vectors that are perpendicular to the longitudinal axis. This project simulated Piezoelectric Micromachined Ultrasonic Transducer (PMUT) with three different material properties i.e. Aluminium Nitride (AlN), Lead zirconate titanate (PZT) and Zinc Oxide (ZnO). Based on the study, it was found that reducing the beam dimensions and increasing the plate size will result in the first mode frequency reduction from  $1.33 \times 10^7$  Hz to  $3.74 \times 10^6$  Hz. Other than that, it was found that AlN PMUT experienced the maximum deflection of 6.3413 to 6.3478  $\mu\text{m}$  when the loads applied in the range of 50 to 200  $\mu\text{N}/\text{m}^2$ . When the piezoelectric material changed to PZT, we obtained the maximum deflections of 0.3771 to 0.3786  $\mu\text{m}$  when the same loads range applied to the PMUT. As for the ZnO PMUT, the maximum deflections obtained were in between 0.1702  $\mu\text{m}$  to 0.1772  $\mu\text{m}$  with the loads are maintained as in the loads applied to the AlN and PZT. This study proved the significant impact of altering the structural dimensions and material properties of PMUTs on their operational characteristics, specifically the first mode frequency and deflection behavior.*

**Keywords:** Aluminium Nitride; Piezoelectric; Zinc Oxide, MEMS PMUT

## 1. INTRODUCTION

Piezoelectric Micromachined Ultrasonic Transducers (PMUTs) represent a cutting-edge class of MEMS-based ultrasonic transducers tailored for high-resolution acoustic imaging of the surroundings. PMUTs use the bending motion of a thin membrane linked with a thin piezoelectric film, whereas solid piezoelectric transducers use the thickness motion of a plate made of piezoelectric ceramic. PMUTs have several advantages over solid piezoelectric ultrasonic transducers, including increased bandwidth, greater support for adjustable geometries, normal acoustic impedance matching to different media, such as water, lower voltage specifications, mixing of different resonant frequencies, and integration potential with supporting electronic circuits, which is especially important for miniaturized high-frequency applications [1].

---

\* Corresponding author: hasnizah@unimap.edu.my

An electric voltage is produced when a material is mechanically deformed, such as by squeezing or tapping. A Piezoelectric crystal is sandwiched between two metal plates. The metal plates then exert mechanical strain on the material, disrupting the balance of the electric charges within the crystal. Compact, low-power transducers as well as transducer arrays that are linked with electronic systems are required for many ultrasonic sensing, actuation, and imaging applications. PMUTs, or piezoelectric micromachined ultrasonic transducers, are thin film flexural transducers with a diaphragm-like structure that may be employed in integrated transducer arrays and are made on silicon substrates [1]. However, some other researchers such as Yongbin Jeong *et al* [2] have also investigated the stress impact to the flexural diaphragm-like structure and proposed an analytical model flexible PMUT device that applied on curved surfaces.

In this work, the performance of PMUT using three different piezoelectric materials namely AlN, PZT and ZnO were investigated and compared. AlN is chosen based on its capability to easily integrated with common integrated circuit and in addition, Chunlong Fei *et al* [3] has written a comprehensive overview of AlN thin films which is including its suitability to be applied in ultrasonic transducer. As for PZT, despite of its environmental concerns, it is still a favourable option due to the high piezoelectric coefficient. An article Deqing Kong *et al* [4] had just recently published, showcasing PZT in their acoustic underwater propulsion system. Finally, ZnO is also selected as one of the option since it is a semiconducting piezoelectric material that has been widely used in the MEMS sensors and actuators, such as in surface acoustic wave (SAW) and thin-film bulk acoustic wave resonator (FBAR) devices.

## 2. METHODOLOGY

Material properties of the three piezoelectric materials used in this study i.e. ZnO, PZT and AlN are shown in Table 1. AlN was chosen in this work even though it has lower piezoelectric coefficients than those of PZT or ZnO because of its great material characteristics such as high elastic modulus, low density, and low dielectric constant, as well as post-CMOS compatible production, make it ideal for a variety of applications [1].

**Table 1** Properties of selected piezoelectric materials

Material	Relative permittivity (Dielectric constant)	Young modulus (GPA)	Density (kg/m <sup>3</sup> )	Coupling factor (k)	Curie temperature (°C)
AlN	-	310	3320	-	-
PZT-4 (PbZrTiO <sub>3</sub> )	1300 – 1475	48 - 135	7500	0.6	365
PZT-5A (PbZrTiO <sub>3</sub> )	1730	48 - 135	7750	0.66	365
ZnO	8.5	210	5600	0.075	-

As for the piezoelectric relative permittivity, the  $d$  matrix of aluminium nitride, AlN, PZT and ZnO are given by the following matrix respectively.

$$d_{ij} = \begin{pmatrix} 0 & 0 & 0 & 0 & 4 & 0 \\ 0 & 0 & 0 & 4 & 0 & 0 \\ -2 & -2 & 5 & 0 & 0 & 0 \end{pmatrix} \text{pC/N.}$$

$$d = \begin{bmatrix} 0 & 0 & 0 & 0 & 584 & 0 \\ 0 & 0 & 0 & 584 & 0 & 0 \\ -171 & -171 & 374 & 0 & 0 & 0 \end{bmatrix} \times 10^{-12} \text{ C/N}$$

$$d = \begin{bmatrix} 0 & 0 & 0 & 0 & -11.34 & 0 \\ 0 & 0 & 0 & -11.34 & 0 & 0 \\ -5.43 & -5.43 & 11.37 & 0 & 0 & 0 \end{bmatrix} \text{pC/N.}$$

Additionally, the resonance frequency is also calculated by using the formula. From the review journal, Eq. 1 is used for the fixed guide beams.

$$f_n = \frac{k_n}{2\pi} \sqrt{\frac{EIg}{wl^4}} \quad (1)$$

In the Eq. 1, cantilever's length is given by  $l$  and  $t$  represents the thickness of layer.  $I$  stand for the moment of inertia;  $A$  represents the area of layer; while  $E$  represents the value of young's modules the  $d_{31}$  state for the piezoelectric constant.

The moment of inertia is calculated by using Eq. 2.

$$I = \left(\frac{wt^3}{12}\right) \quad (2)$$

Other than that, the force constant of any fixed-guided beam is determined by using Eq. 3.

$$k = \frac{12El}{t^3} \quad (3)$$

Each spring shared 1/nth of the total force load when a force is applied to a plate supported by  $n$  cantilevers of identical size and force constants. The total force constant that the spring is subjected to is  $nk$ .

The corresponding force constant for a plate supported by four fixed guided beams is calculated by using Eq. 4 [6];

$$k = 4\left(\frac{Ewt^3}{t^3}\right) \quad (4)$$

Thus, resonant frequency for a plate supported by four fixed guided beams is given by Eq. 5 [6];

$$f_n = \frac{k}{2\pi} \sqrt{\frac{Et^2}{12\rho l^4}} \quad (5)$$

While for rectangular flat plate or membrane with short edge, long edge and thickness, the resonant frequency is given by Eq. 6.

$$f_n = \frac{k_1}{2\pi} \sqrt{\frac{Dg}{wa^4}} \tag{6}$$

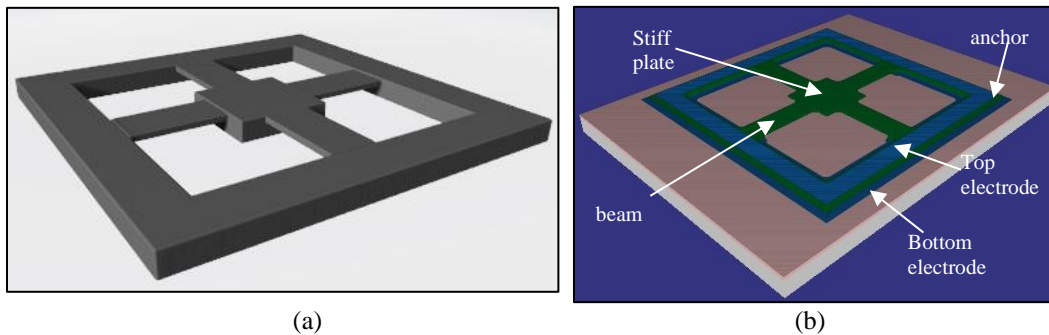
### 2.1 Modelling Fixed-Guide Layout

Flexural beams are categorised by the combination of two mechanical boundary conditions with which they are associated. For example, a fixed-free beam, also known as a cantilever, is a beam that is fixed at one end and free at the other. Fixed-free (cantilevers), fixed-fixed (bridges), and fixed-guided beams are the most common types of beams seen in MEMS research [6].

Fixed-guided springs are frequently employed to support and facilitate the translation of rigid plates. A plate is frequently supported by two or more of these beams. One end of the beam is fixed in these circumstances, and all degrees of freedom are limited. Because it is attached to the stiff translational plate, which remains parallel to the substrate during authorised plate movement, the other end of the spring can move vertically but not angularly. Figure 1 (a) shows the design of the piezoelectric layer while Fig. 1(b) shows the two electrodes that sandwiched piezoelectric material. This project used Molybdenum for top and bottom electrodes. This model is created based on the 2D drawing from the Blueprint as shown in Fig. 2. Table 2 summarizes the dimensions of each layer used in this model.

**Table 2** Design dimension

	Length, <i>l</i> (μm)	Width, <i>w</i> (μm)	Thickness, <i>t</i> (μm)
Stiff Plate	20.0	10	1.0
Beam	18.0	10	1.0
Anchor	80.0	10	1.0
Bottom Electrode (Molybdenum)	84.0	14	1.0
Top Electrode (Molybdenum)	76.0	6	1.0



**Figure 1.** (a) Schematic of piezoelectric without top and bottom of electrode (b) Schematic of piezoelectric that sandwiched with electrodes

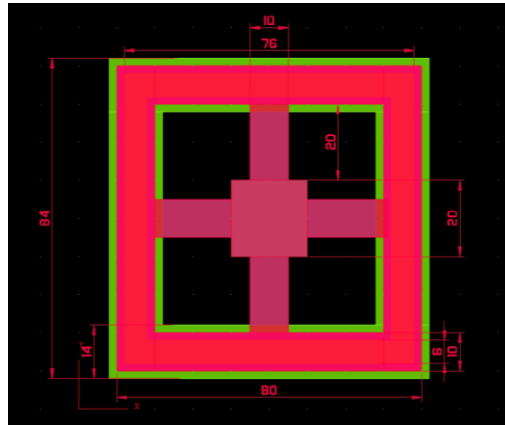


Figure 2. 2D drawing using Blueprint

### 3. RESULTS AND DISCUSSION

This chapter discusses the results from simulations that have been done to complete this project. All the results will be analysed and conclude to identify the material with excellent performance.

#### 3.1 Design and Fabrication Process

This work started with designing the layout of the Si-based PMUT using Aluminium Nitride (AlN). Then, the fabrication process steps were defined by using the IntelliFAB and Fabsim in the Intellisuite. IntelliFAB or process visualization allows user to create and debug the process flow and mask set before entering the clean room. It also allows user to make virtual prototypes to save costly fabrication mistakes. Before the process proceeded to Fabsim, this project needed to go through IntelliFAB. All the fabrication process steps must be properly defined in here. Figure 2 shows all the process steps required for this project. Fabrication process step is started by defining the substrate used in the PMUT namely Si in this project. There are in total 40 process steps in order to create a PMUT structure as shown in Figure 1(b).

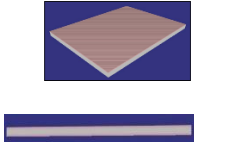
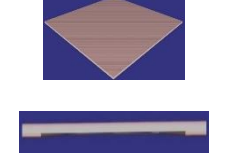
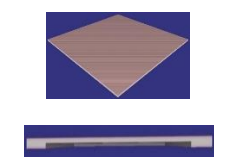

No	Type	Material	Process	Process Option
1	Definition	Si	Czochralski	
2	Deposition	SiO <sub>2</sub>	Bulk	Conformal Deposition
3	Deposition	PR_AZ5214	Spin	Conformal Deposition
4	Exposure	UV	Contact	
5	Etch	SiO <sub>2</sub>	RIE	Partial Etching
6	Etch	Si	RIE	Partial Etching
7	Etch	PR_AZ5214	Wet	Partial Etching
8	Deposition	PR_AZ5214	Spin	Conformal Deposition
9	Exposure	UV	Contact	
10	Etch	SiO <sub>2</sub>	RIE	Partial Etching
11	Etch	PR_AZ5214	Wet	Partial Etching

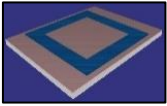

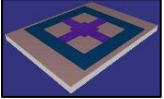

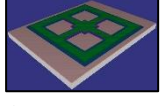
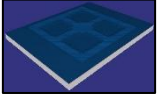
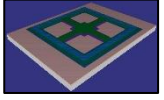
12	Deposition	Mo	Bulk	Conformal Deposition
13	Deposition	PR_AZ5214	Spin	Conformal Deposition
14	Exposure	UV	Contact	
15	Etch	Mo	Wet	Partial Etching
16	Etch	PR_AZ5214	Wet	Partial Etching
17	Deposition	Si3N4	PECVD	Planarization
18	Deposition	PR_AZ5214	Spin	Conformal Deposition
19	Exposure	UV	Contact	
20	Etch	Si3N4	RIE	Partial Etching
21	Etch	PR_AZ5214	Wet	Partial Etching
22	Deposition	PR_AZ5214	Spin	Conformal Deposition
23	Exposure	UV	Contact	
24	Etch	Si3N4	Wet	Partial Etching
25	Etch	PR_AZ5214	Wet	Partial Etching
26	Deposition	AlN	Sputter	Planarization
27	Deposition	PR_AZ5214	Spin	Conformal Deposition
28	Exposure	UV	Contact	
29	Etch	AlN	RIE	Partial Etching
30	Etch	PR_AZ5214	Wet	Partial Etching
31	Deposition	Mo	Bulk	Conformal Deposition
32	Deposition	PR_AZ5214	Spin	Conformal Deposition
33	Exposure	UV	Contact	
34	Etch	Mo	Wet	Partial Etching
35	Etch	PR_AZ5214	Wet	Partial Etching
36	Etch	Si3N4	RIE	Sacrificial
37	Deposition	PR_AZ5214	Spin	Conformal Deposition
38	Exposure	UV	Contact	
39	Etch	SiO <sub>2</sub>	RIE	Partial Etching
40	Etch	Si	RIE	Sacrificial

**Figure 2.** Fabrication process setup for AlN in IntelliFAB

Table 3 summarizes the fabrication steps of PMUT using 3D and cross-section view of each step. The same process steps will also be applied to the PMUT that using both PZT and ZnO materials.

**Table 3** Fabrication steps of the PMUT using AlN as a piezoelectric material

<p>(1) Definition of Si substrate as in Step 1 in the fabrication process.</p>	 <p>(2) Deposition of SiO<sub>2</sub> layer as using conformal</p>	 <p>(3) Patterning of SiO<sub>2</sub> layer using the first mask.</p>	 <p>(4) Etching process of the exposed Si substrate</p>	 <p>(5) Deposition of Mo layer as the bottom</p>
--	---	--	---	---

	deposition.			electrode layer
				
(6) Mo patterning process using the 2 <sup>nd</sup> mask.	(7) Deposition of nitride layer using planarization process.	(8) Patterning of Si <sub>3</sub> N <sub>4</sub> layer using the 3 <sup>rd</sup> mask.	(9) Deposition of piezoelectric layer (AlN, PZT or ZnO)	(10) Patterning of piezoelectric layer using the 4 <sup>th</sup> mask.
 (11) Deposition of Mo layer as the top electrode layer			 (12) Patterning of Mo using the 5 <sup>th</sup> mask.	

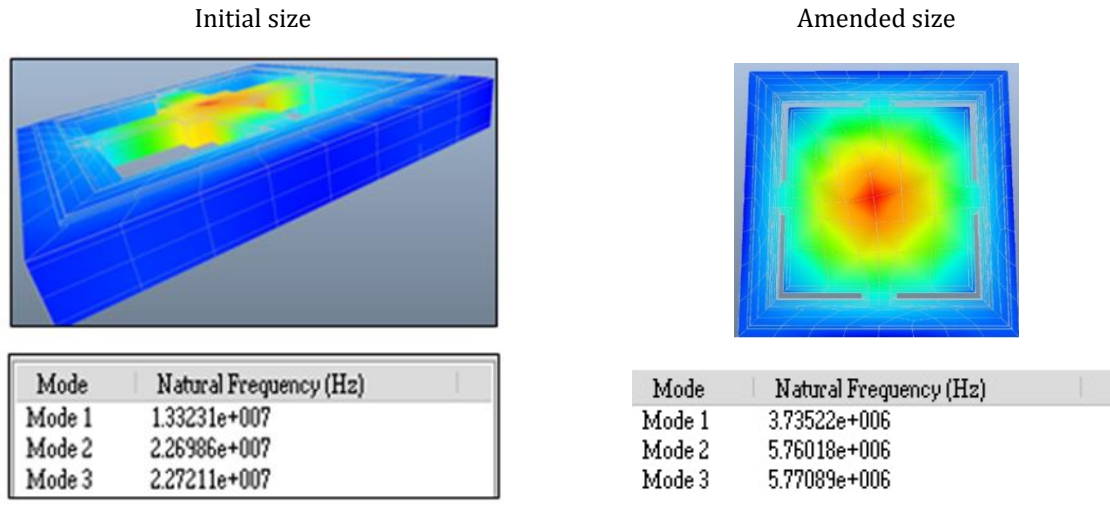
### 3.2 Simulation results

Equation 5 shows how the resonant frequency of the PMUT has also relation to the dimension on the beam and plate size. Due to that reason, a simulation has been run to investigate this issue and Table 4 shows the changes that we made to the PMUT size.

**Table 4** Changes in the PMUT dimension

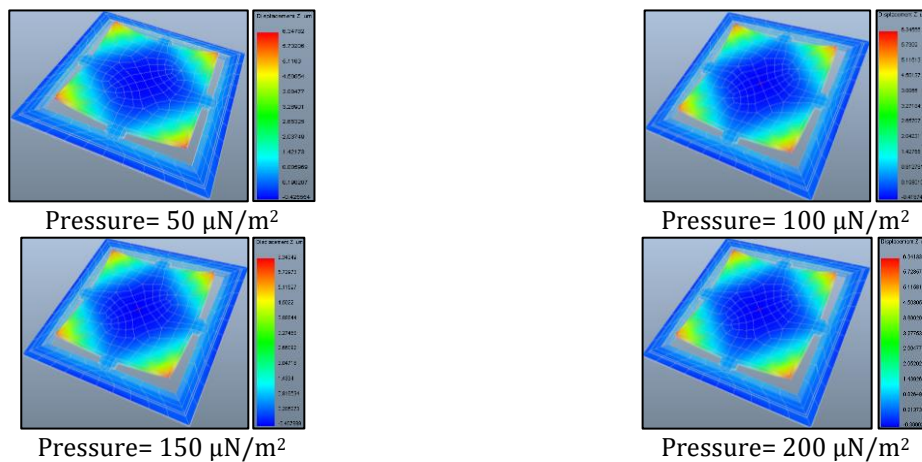
	Initial size			Amended size		
	Length, <i>l</i> (μm)	Width, <i>w</i> (μm)	Thickness, <i>t</i> (μm)	Length, <i>l</i> (μm)	Width, <i>w</i> (μm)	Thickness, <i>t</i> (μm)
Stiff Plate	20.0	10	1.0	36	10	1.0
Beam	18.0	10	1.0	2	10	1.0
Anchor	80.0	10	1.0	80.0	10	1.0
Bottom Electrode (Molybdenum)	84.0	14	1.0	84.0	14	1.0
Top Electrode (Molybdenum)	76.0	6	1.0	76.0	6	1.0

As shown in Fig. 3, the resonant frequency of the PMUT was reduced when the beam length reduced and the plate size increased. In the first mode of resonant frequency, the frequency was reduced from  $1.33 \times 10^7$  Hz to  $3.74 \times 10^6$  Hz.



**Figure 3.** The effect of beam and plate sizes to the resonant frequency

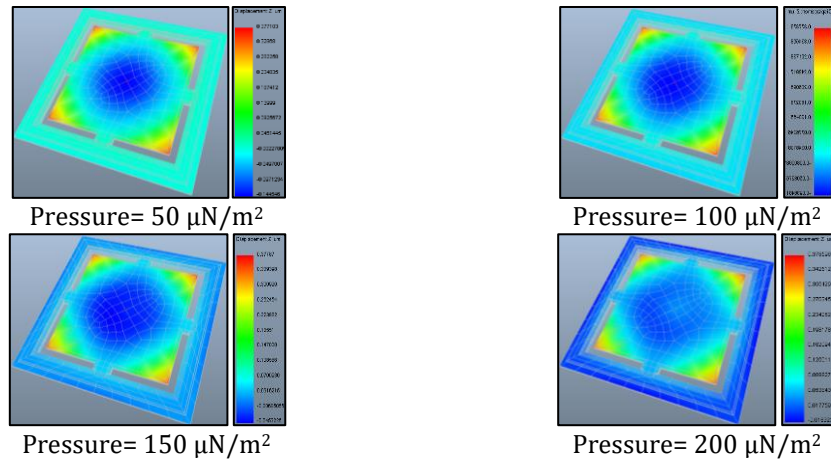
Pressure was then applied and varied to the PMUT structure in order to perform study of the performance of PMUT in the different piezoelectric materials. Figure 4 shows the deflection experienced by an AlN PMUT when the pressure applied in between 50 to 200  $\mu\text{N}/\text{m}^2$ . It was found that the maximum deflections were 6.3413  $\mu\text{m}$ , 6.3435  $\mu\text{m}$ , 6.3457  $\mu\text{m}$  and 6.3478  $\mu\text{m}$  when the pressure applied were 50  $\mu\text{N}/\text{m}^2$ , 100  $\mu\text{N}/\text{m}^2$ , 150  $\mu\text{N}/\text{m}^2$  and 200  $\mu\text{N}/\text{m}^2$  respectively.



**Figure 4.** Deflection on the AlN PMUT structure when the load is varied

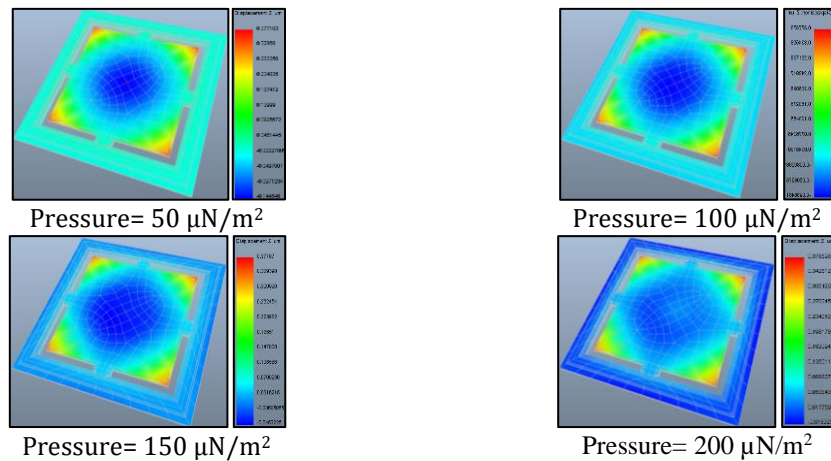
Then, the same process was repeated with the piezoelectric material is changed to PZT. Figure 5 shows the deflection on the PZT PMUT when the pressure applied in between 50 to 200  $\mu\text{N}/\text{m}^2$ . The maximum deflections were 0.3771  $\mu\text{m}$ , 0.3774  $\mu\text{m}$ , 0.3779  $\mu\text{m}$  and 0.3786  $\mu\text{m}$  when the pressure applied were 50  $\mu\text{N}/\text{m}^2$ , 100  $\mu\text{N}/\text{m}^2$ , 150  $\mu\text{N}/\text{m}^2$  and 200  $\mu\text{N}/\text{m}^2$  respectively.





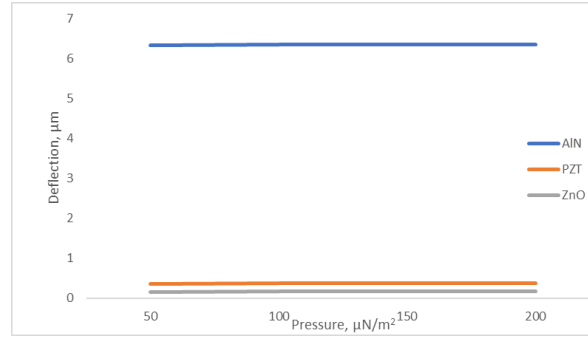
**Figure 5.** Deflection on the PZT PMUT structure when load is varied

Figure 6 shows the deflection on the PMUT when the piezoelectric material is changed to ZnO and the same pressures were applied as in the previous simulation. The maximum deflections were 0.1702  $\mu\text{m}$ , 0.1725  $\mu\text{m}$ , 0.1749  $\mu\text{m}$  and 0.1772  $\mu\text{m}$  when 50  $\mu\text{N}/\text{m}^2$ , 100  $\mu\text{N}/\text{m}^2$ , 150  $\mu\text{N}/\text{m}^2$  and 200  $\mu\text{N}/\text{m}^2$  load were applied to the structure respectively.



**Figure 6.** Deflection on the ZnO PMUT when the load is varied

From graph plotted in Fig. 7, it shows that the highest deflections obtained by the AlN then following by the PZT and ZnO. However, there were no significant changed occurred when the pressure varied from 50 to 200  $\mu\text{N}/\text{m}^2$ . This probably happened due to the insignificant changes in the load variation.



**Figure 7.** Max deflection on PMUT with AlN, PZT and ZnO as the piezoelectric material

#### 4.0 CONCLUSION

As a conclusion, the dimensions of the beams and plate have significant effect to the resonant frequency. The shorter the beam, the smaller the resonant frequency of the PMUT. The result obtained from the simulation shows a good agreement with the theory. However, it was found that the max deflection of the PMUT was incorrect for the AlN. AlN material properties as shown in Table 1 showed that it has the highest Young's Modulus value as compared to PZT and ZnO and theoretically, deflection can be calculated by taking the double integral of the Bending Moment Equation,  $M(x)$  divided by Young's Modulus  $E$  multiply by Moment of Inertia,  $I$ . It means that AlN is expected to obtain the lowest deflection than PZT and ZnO. This probably happened due to insufficient number of nodes used during simulation. Further study will be done to obtain more accurate deflections results for the PMUT using all three piezoelectric materials.

#### ACKNOWLEDGEMENT

Thank you to the Faculty of Electronic Engineering Technology of UniMAP for providing simulation facilities used in this work.

#### REFERENCES

1. "An Introduction to MEMS", PRIME Faraday Partnership, Loughborough University (2002)
2. Yongbin Jeong, Jan Genoe, Pieter Gijsenbergh, Jeremy Segers, Paul L. Heremans, and David Cheyens. *Journal of Microelectromechanical Systems*, Vol. **30**, No. 1 (February 2021)
3. Chunlong Fei, Xiangli Liu, Benpeng Zhu, Di Li, Xiaofei Yang, Yintang Yang, and Qifa Zhou. *Nano Energy*, Vol. **51** (2018) pp. 146-161
4. Deqing Kong, Takumi Hirata, Yimeng Wang, Fei Li, Minoru Kuribayashi Kurosawa, Manabu Aoyagi. *Sensors and Actuators A: Physical*, Vol. **359** (2023), pg. 114502.
5. H. Li, C. Tian, and Z. D. Deng. *Appl. Phys. Rev.*, Vol. **1**, no. 4 (2014)
6. Chang Liu, "Foundations of MEMS, 2<sup>nd</sup> edition", Pearson Education (2012)
7. Wang. M., Zhou Y. *Microsystem Technologies*. Vol. **23** (2017), pp. 1761-1766
8. Agnieszka Kołodziejczak-Radzimska and Teofil Jesionowski. *Materials*, Vol. **7**(4) (2014), pp. 2833-2881
9. Thomas M. Adams, Richard A. Layton, "Introductory MEMS, Fabrications and Applications", Springer Science+Business Media, LLC (2010)